10. D. O. Burgess, M. J. Sharp, D. W. F. Mair, J. A. Dowdeswell, T. J. Benham, *J. Glaciol.* **51**, 219 (2005).
11. G. Kaser, J. G. Cogley, M. B. Dyurgerov, M. F. Meier, A. Ohmura, *Geophys. Res. Lett.* **33**, L19501 (2006).
12. M. F. Meier, A. Post, *J. Geophys. Res.* **92**, 9051 (1987).
13. M. B. Dyurgerov, M. F. Meier, *Occasional Paper No. 58*, (Institute of Arctic and Alpine Research, Univ. of Colorado, Boulder, CO, 2005).
14. We have revised the total area of GIC from 785×10^3 km^2 to 763×10^3 km^2 because of an overestimate of the glaciers peripheral to Greenland Ice Sheet. This adjustment has been applied throughout.
15. S. C. B. Raper, R. J. Braithwaite, *Nature* **439**, 311 (2006).
16. S. Rahmstorf, *Science* **315**, 368 (2007).
17. D. B. Bahr, M. F. Meier, *Water Resour. Res.* **36**, 495 (2000).
18. D. B. Bahr, *Water Resour. Res.* **33**, 1669 (1997).
19. Because there are many areas without complete inventories of GIC sizes, we used two estimation processes to fill gaps. First, we used an estimate of the probability of the number of glaciers greater than a certain area versus that area, based on percolation theory and on known size distribution relations. The error in this process for a global total was estimated at about 13% (*13*). Next, we estimated the thickness of GIC based on power-law scaling with glacier area. Without sufficient independent data, it is difficult to estimate the error in the method. We estimated that the error in calculating thicknesses and thus volumes from area values is on the order of 25% for global aggregates (*13*) but far greater, on the order of 50%, for individual ice masses.
20. M. F. Meier, D. B. Bahr, M. B. Dyurgerov, W. T. Pfeffer, *Geophys. Res. Lett.* **32**, L17501 (2005).
21. This work was supported by NSF grants OPP 0327345, OPP 0425488, and EAR 0549566; NASA grants NGT5-155 and NAG5-13691; and a Marie Curie International Fellowship within the 6th European Community Framework Program. We thank three anonymous reviewers for their critical reading of the manuscript.

The Southern Ocean Biological Response to Aeolian Iron Deposition

Nicolas Cassar,[1]* Michael L. Bender,[1] Bruce A. Barnett,[1] Songmiao Fan,[2] Walter J. Moxim,[2] Hiram Levy II,[2] Bronte Tilbrook[3]

Biogeochemical rate processes in the Southern Ocean have an important impact on the global environment. Here, we summarize an extensive set of published and new data that establishes the pattern of gross primary production and net community production over large areas of the Southern Ocean. We compare these rates with model estimates of dissolved iron that is added to surface waters by aerosols. This comparison shows that net community production, which is comparable to export production, is proportional to modeled input of soluble iron in aerosols. Our results strengthen the evidence that the addition of aerosol iron fertilizes export production in the Southern Ocean. The data also show that aerosol iron input particularly enhances gross primary production over the large area of the Southern Ocean downwind of dry continental areas.

The rate of organic matter export from the surface waters of the Southern Ocean has an important impact on distributed properties of the environment. First, it influences the residual nutrient burden of waters that flow northward in the subsurface to supply nutrients to much of the extrapolar ocean (*1*). Second, carbon export removes CO_2 from surface waters, thereby influencing the atmospheric CO_2 concentration over both glacial-interglacial and anthropogenic time scales. There is compelling evidence that iron supply from a number of sources (such as coastal sediments, aerosols, upwelling, ice melting, and enhanced mixing over high topography) influences rates of both gross production and carbon export by Southern Ocean ecosystems. Ocean color data, for example, show that biomass is elevated downwind of aeolian iron sources, and extraordinary "patch" experiments have shown that iron addition enhances primary production

and new production in several representative regions (*2*).

To understand the potential for aeolian iron fertilization, we compared a large number of net community production (NCP) measurements in the Southern Ocean (*3*, *4*) to a modeled Fe deposition (*5*). NCP and gross primary production (GPP) are calculated as the production rates required to maintain the observed biological O_2 supersaturation (derived from O_2/Ar) and O_2 triple-isotope anomaly against equilibration by gas exchange (parameterized in terms of wind speed) (*6*). NCP from O_2 is the stoichiometrically equivalent rate of organic carbon production in excess of respiration; it approximates carbon export from the mixed layer. Our data set establishes the pattern of this fundamental rate process in the Southern Ocean at a scale heretofore accessed only for chlorophyll, which reflects biomass. We implemented these methods with samples of water from the upper-ocean mixed layer. Samples were collected by us or collaborators on cruises of opportunity and returned to the laboratory for analysis; in this way, it was possible to assemble a very large data set.

Our approach to determining NCP and GPP has distinct attributes and limitations. The method accesses production over times on the order of 1 week, corresponding to the mixed-layer depth divided by the piston velocity. We as-

sumed steady-state mixed-layer depth and productivity (clearly a simplification). We ignored exchange between the mixed-layer and underlying waters. The analysis of Wang *et al.* (*7*) suggests that, in the Polar Front Zone and the Subantarctic Zone, this process is of minor importance in the summer and in the spring. When the flux of O_2 is into the ocean, we report negative values of NCP. Although we refer to the air-sea biological O_2 flux as NCP, we were unable to determine whether negative values reflect net heterotrophy in the mixed layer or upwelling of O_2-undersaturated waters.

Figure 1 shows summer NCP values superimposed on Southern Ocean properties (*8*). Most of the Southern Ocean can be considered a high-nutrient low-chlorophyll region, with the caveat that the area north of the Antarctic Polar Front (APF) is depleted in silicate during summertime. The strong westerlies around the Antarctic continent drive a northward Ekman transport of nutrient-rich circumpolar deep waters that upwell south of the APF. From the south, the Antarctic Zone lies between the Southern Boundary of the Antarctic circumpolar current and the APF, the Polar Frontal Zone stretches from the APF to the Subantarctic Front, and the Subantarctic Zone extends from the Subantarctic Front to the Subtropical Front. The Subtropical Front is the boundary between the warm and salty subtropical waters and the relatively cooler and fresher waters of the Southern Ocean. The summertime chlorophyll distribution is shown by the background colors of the map (Fig. 1).

We observed that, in general, NCP rises toward the north (Figs. 1 and 2), with considerable spatial heterogeneity. Visual inspection, along with the statistical analysis of Reuer *et al.* (*4*), shows that NCP is weakly correlated with climatological satellite chlorophyll estimates. Our results also show higher NCP and GPP in the spring than in the summer over most of the Southern Ocean (*9*) (Fig. 2). Our approach underestimates NCP in upwelling areas, where mixing to the surface of O_2-depleted waters lowers the biological O_2 supersaturation. For this reason, the apparent poleward decrease in NCP could partially be driven by upwelling of upper circum-

[1]Department of Geosciences, Princeton University, Princeton, NJ 08544, USA. [2]Geophysical Fluid Dynamics Laboratory/National Oceanic and Atmospheric Administration, Post Office Box 308, Princeton, NJ 08542, USA. [3]Commonwealth Scientific and Industrial Research Organisation (CSIRO) Marine and Atmospheric Research and Antarctic Climate and Ecosystem Cooperative Research Center, Hobart, Tasmania 7001, Australia.

*To whom correspondence should be addressed. E-mail: ncassar@princeton.edu

polar deep water south of the APF. However, we believe that part of this poleward decrease accurately reflects the gradient in mixed-layer fertility because chlorophyll concentration, as well as our $^{17}\Delta$-based estimates of GPP (which are less affected by upwelling), show a similar trend (Fig. 2).

We considered three properties that, individually and in combination, influence spatial variability of summertime Southern Ocean productivity: Si(OH)$_4$, light, and iron. Si(OH)$_4$ undoubtedly limits diatom production at certain times but cannot account for the pattern of GPP and NCP that we observed: It is replete only in southern waters, but production is highest in the north (4). In addition, because of diatom Si:C plasticity, limitation of Si(OH)$_4$ uptake does not necessarily entail carbon-specific growth limitation (10). The mixed layer is sometimes light-limited because deep mixed layers, with lower mean irradiance, are typical of the Southern Ocean. However, a comparison of our summer NCP measurements to climatological photosynthetically active radiation within the mixed layer shows no statistically significant correlation (fig. S1).

Iron might account for meridional variability in open ocean production in one of three ways. First, if the source of iron is upwelled subsurface waters, production should be elevated near the zone of upwelling—mainly around and south of the APF. Indeed, there is some evidence for higher production at the APF. However, as water upwells south of the APF and flows northward in the Ekman Drift, we do not observe the predicted decrease in production, which theoretically would be caused by removal of iron by scavenging and carbon export. Furthermore, studies from the Australian and Pacific sectors of the Southern Ocean agree that the mixed-layer Fe concentration increases, rather than decreases, toward the north (11–13). This iron increase to the north is accompanied by rising relative variable fluorescence as measured by fast repetition rate fluorometry (14, 15). Relative variable fluorescence is positively correlated to in situ Fe concentration in the Southern Ocean (14). In addition, phytoplankton communities north of the APF do not respond as strongly in Fe enrichment experiments as the ones south of the APF (15).

Second, if the source of iron is seasonal or annual aerosol input, production should be correlated to long-term average Fe deposition. Given a plausible residence time on the order of 5 months (calculated for the Subantarctic Zone assuming soluble iron deposition = 0.06 µmol m^{-2} day^{-1}, mixed-layer depth = 30 m, and mixed-layer [Fe] = 0.3 nmol kg^{-1}), the dissolved Fe concentration will reflect aerosol deposition somewhat upstream of the sampling point, a complication we neglect here. In Fig. 3A, we plot NCP versus the annual iron deposition rate at the sampling location computed by Fan et al. (5). Their model, driven by analyzed meteorological properties, simulates chemical changes occurring in aerosols that increase Fe solubility with atmospheric transport time (Fig. 4A). This

increase in Fe solubility exerts a first-order control on aerosol Fe input to the oceans (16). Relative to a model assuming that a constant fraction of iron dissolves, models invoking chemical transformations predict diminished soluble Fe addition near dust sources and enhanced delivery in remote regions (Fig. 4B). Uncertainties in the entrainment rates of dust in the source areas and the fraction of soluble iron in settling aerosols introduce important errors into rates of soluble iron deposition simulated by the model. There is clearly a strong correlation between NCP and annual Fe deposition ($r = 0.60$, df = 381; Fig. 3A).

Third, if the source of iron is synoptic-scale deposition, production should be correlated with the deposition rate during some recent period. The correlation coefficient between NCP and soluble iron deposition is a maximum when iron deposition is averaged for a period of 14 days before sampling ($r = 0.53$, df = 381; Fig. 3B), decreasing only slightly with longer averaging times (6). This period may be shorter than the average residence time. Nevertheless, synoptic-scale events would lead to variability of about 25% in the ambient iron concentration given transient doublings and halvings of the soluble iron input with a 30-day cycling time. Such changes appear feasible based on the comparison of average Fe deposition at sampling sites during the 2-week period before collection and the average

annual Fe deposition at the sites (fig. S2), and the variability would of course be greater if the residence time were <5 months. Fe excursions might raise NCP by inducing transient increases in phytoplankton growth that would eventually be curtailed as grazers respond. Alternatively, recently added iron might be more available to phytoplankton than iron that has resided for a longer time in the mixed layer. A large proportion of Fe in the mixed layer is organically chelated (17, 18), and the bioavailability of this ligand-complexed Fe is poorly understood (19). Similar analyses demonstrate the influence of soluble Fe deposition on GPP as well (fig. S3).

Thus, our data are compatible with either annual iron deposition or synoptic-scale iron deposition that has a significant influence on variability of NCP, as well as GPP, in the Southern Ocean. Statistical tests confirm the link between increasing iron deposition and increasing NCP and GPP (6). Some of the variability in NCP versus Fe deposition can be explained by other sources of Fe (such as meltwater, sedimentary, and upwelling sources), variable phytoplankton Fe:C quotas, light and silicate limitations, parameterization of the atmospheric Fe dissolution kinetics, aeolian transport model errors, and wind parameterization of the piston velocity.

To explore the potential and nature of atmospheric Fe fertilization, we performed a model
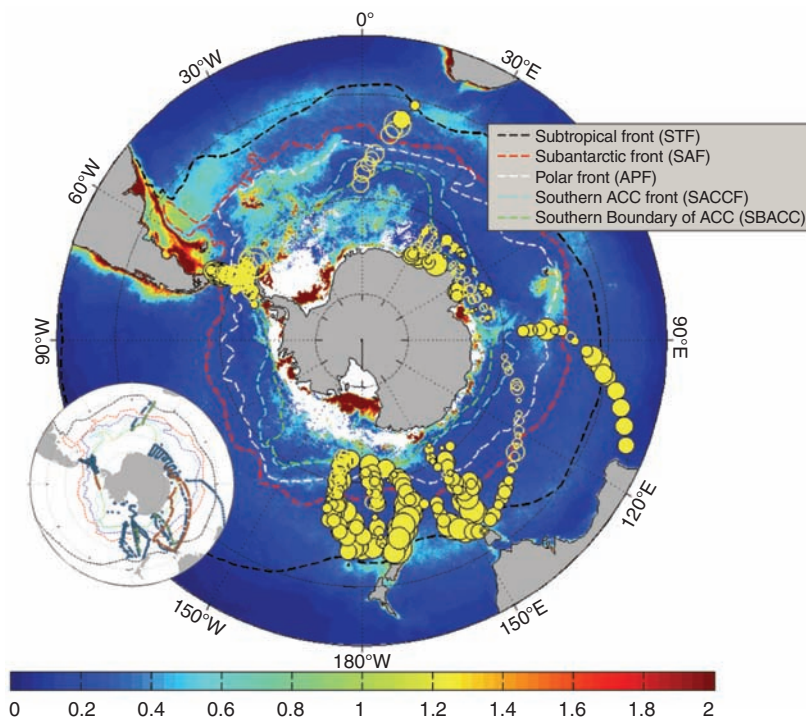
Fig. 1. Austral summer NCP measurements in the Southern Ocean. Yellow circles indicate locations of summertime O$_2$/Ar samples from which we calculated air-sea O$_2$ fluxes and NCP values. Open circles denote O$_2$-undersaturated waters and O$_2$ fluxes into the ocean. Closed circles reflect net autotrophy, with the circle size proportional to its magnitude. The largest filled circle represents 168 µmol O$_2$ m^{-2} day^{-1}. Sea-Viewing Wide Field-of-View Sensor (SeaWiFS) summer chlorophyll a climatology is also shown (color bar, bottom, in mg m^{-3}). (Inset) Color-coded sampling sites with summer, spring, and fall in blue, green, and orange, respectively. Dashed lines indicate the climatological locations of fronts that separate the main water masses associated with the Antarctic circumpolar current (ACC) (35).
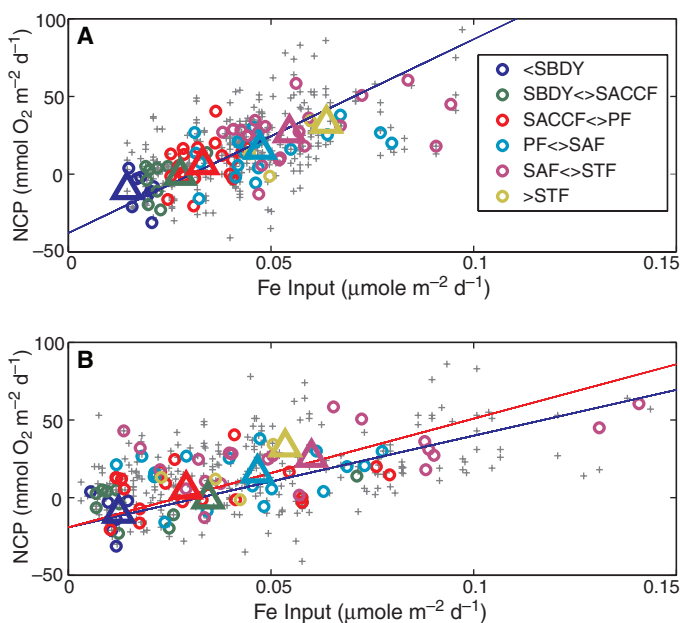
II least-squares bisector regression analysis (20) to calculate the Fe/C_{org} ratio (aerosol Fe input/ NCP) implied by our data (Fig. 3B). We adopted an O_2/C molar photosynthetic quotient of 1.4 for NCP (i.e., NCP is assumed to be mostly nitrate-derived) (21). The resulting Fe/C_{org} ratio for the spring and summer seasons is 2.5 µmol mol^{-1}. This number is markedly similar to the oceanic Fe/C ratios in Southern Ocean phytoplankton (22) (1.5 and 2.1 µmol mol^{-1} in the Ross Sea and Drake Passage, respectively). For comparison, Fe:C in laboratory cultures of *Thalassiosira oceanica* varies between 2.5 to 34 µmol mol^{-1} depending on Fe availability (23).

In the Southern Ocean, where Fe is highly limiting, phytoplankton species are at the lower end of this range (24–28). Deriving our estimates for the cellular Fe quota based on NCP is reasonable if, in the mixed layer, Fe is stoichiometrically cycled along with organic carbon, rather than independently exported (28). Stoichiometric cycling is supported by the Fe/C remineralization ratio, which is also about 2 µmol mol^{-1} (22). Hence, our results show that photoautotrophs may rely on aeolian input of Fe over a broad area of the Southern Ocean.

Our work, together with other recent studies, provides a comprehensive picture of the ways in which iron fertilization and iron limitation influence the biomass and fertility of Southern Ocean ecosystems. There are five sources of bioavailable iron to surface waters of the Southern Ocean. First, melting of sea ice can release accumulated iron that contributes locally to springtime blooms along the ice edge (29). Second, the release of dissolved iron or resuspension of sediments can supply iron to waters overlying shallow sea floor, accounting for high productivity in continental shelf environments (along the Antarctic coast, for example) (30). Third, upwelling supplies iron and accounts for elevated productivity in some areas of the APF (31) and along the continental slope. Fourth, vertical mixing, induced by rough bottom topography, supplies iron to surface waters and enhances productivity in regions such as the Scotia Sea east of the Drake Passage, and the Kerguelen Plateau in the center of the Indian Antarctic sector (32). Finally, as we discuss, delivery of soluble iron by aerosol deposition supplies that element to the Southern Ocean, particularly areas downwind of substantial dust sources, accounting for elevated chlorophyll and/or productivity to the east of Patagonia and to the south and southwest of Australia, New Zealand, and Africa. Regions lacking all sources are the least fertile in the Southern Ocean, despite their high burdens of NO_3^-, PO_4^{3-}, and $Si(OH)_4$. These include waters overlying the Enderby Abyssal Plain (western Indian sector), South Indian Basin (eastern Indian sector), and the Bellingshausen abyssal Plain (Pacific sector), all in the Antarctic Zone of the Southern Ocean.

Both data and models support the idea that the flux of dust to the Southern Ocean was much higher during the last ice age than during the present or preindustrial times (33). In the Subantarctic region, lower $\delta^{15}N$ of sedimentary nitrogen in glacial sediments (34), along with more rapid biogenic SiO_2 accumulation, indicates higher rates of export production. Increased iron delivery is certainly a plausible explanation for faster export. According to the model of Robinson *et al.* (34), the resulting depletion of subantarctic waters in nutrients and TCO_2 would have led to an atmospheric CO_2 drawdown of up to 40 parts per million, accounting for nearly half the glacial lowering of atmospheric CO_2. Our work shows that delivery of

Fig. 2. Zonally averaged seasonal and regional gradient in (**A**) O_2/Ar-derived NCP, (**B**) oxygen triple isotope–derived GPP (mmol m^{-2} day^{-1}) from available measurements, and (**C**) Fe deposition (µmol m^{-2} year^{-1}) from corresponding model grid boxes. Standard error bars are also shown when available. STF, Subtropical Front; SAF, Subantarctic Front; PF, Antarctic Polar Front (APF); SACCF, Southern ACC Front; SBDY, southern boundary of the ACC.
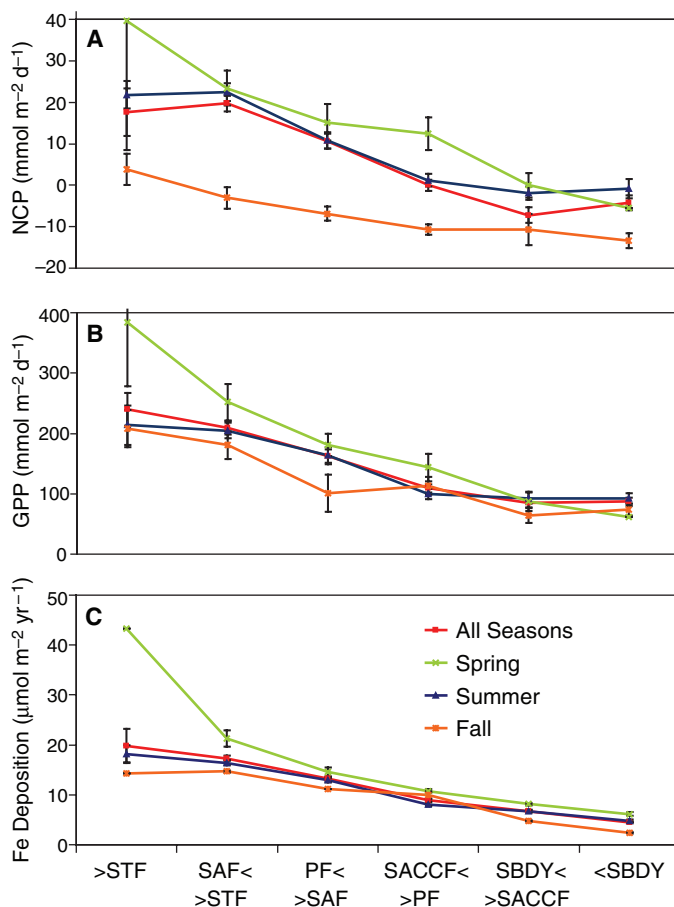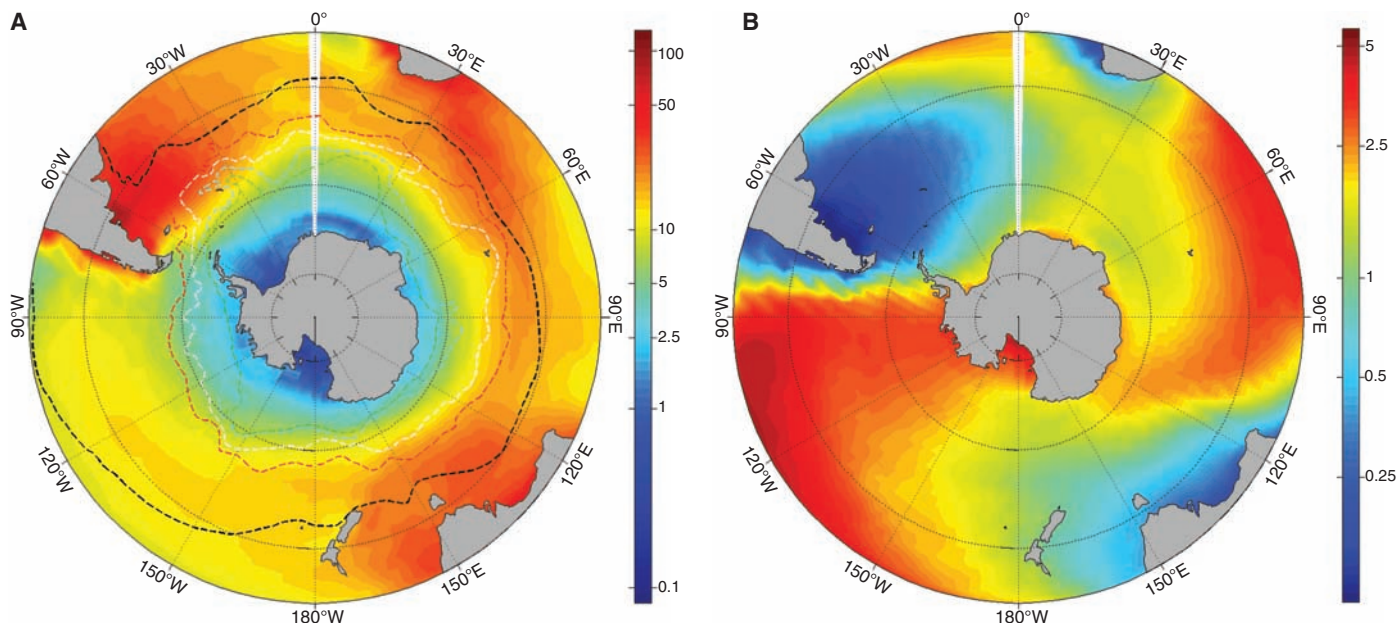

Fig. 3. Spring (16%) and summer (84%) NCP measurements versus corresponding modeled annual (**A**) and 2-week (**B**) Fe deposition rates. Gray pluses, circles, and triangles represent individual observations, regional averages for each transect, and regional averages of all samples, respectively. The blue line represents a model II least-squares bisector regression analysis. The red line represents an Fe requirement of 1.4 µM Fe/MO$_2$ [compatible with Sunda's (22) Southern Ocean phytoplankton's Fe:C ratio estimate and a photosynthetic quotient of 1.4 (21)].

Fig. 4. (A) Annual deposition fluxes of dissolved Fe to the ocean based on the Fan *et al.* (*5*) two-step solubility process (μmol m^{-2} year^{-1}). **(B)** Ratio of fluxes shown in (A) and a constant 5% Fe solubility model.

airborne Fe increases production of subantarctic waters, strengthening the link between enhanced Fe delivery and lower CO_2 during the ice ages. Our work also underscores the importance of understanding the implications of the large change in dust transport to the ocean simulated for the coming centuries (*33*).

References and Notes

1. J. L. Sarmiento, N. Gruber, M. A. Brzezinski, J. P. Dunne, *Nature* **427**, 56 (2004).
2. P. W. Boyd *et al.*, *Science* **315**, 612 (2007).
3. M. B. Hendricks, M. L. Bender, B. A. Barnett, *Deep-Sea Res. I* **51**, 1541 (2004).
4. M. K. Reuer, B. A. Barnett, M. L. Bender, P. G. Falkowski, M. B. Hendricks, *Deep-Sea Res. I* **54**, 951 (2007).
5. S. M. Fan, W. J. Moxim, H. Levy, *Geophys. Res. Lett.* **33**, L07602 (2006).
6. Materials and methods are available as supporting material on *Science* Online.
7. X. J. Wang, R. J. Matear, T. W. Trull, *J. Geophys. Res. Oceans* **106**, 31525 (2001).
8. We include only springtime and summertime data in our discussion. Although fall data strengthen our conclusions, we omitted these results from our analysis because mixed-layer oxygen supersaturation can be influenced by entrainment of undersaturated subsurface waters.
9. M. L. Dickson, J. Orchardo, *Deep-Sea Res. II* **48**, 4101 (2001).
10. D. M. Nelson, M. A. Brzezinski, D. E. Sigmon, V. M. Franck, *Deep-Sea Res. II* **48**, 3973 (2001).
11. P. N. Sedwick, P. R. Edwards, D. J. Mackey, F. B. Griffiths, J. S. Parslow, *Deep-Sea Res. I* **44**, 1239 (1997).
12. H. J. W. de Baar *et al.*, *Mar. Chem.* **66**, 1 (1999).
13. C. I. Measures, S. Vink, *Deep-Sea Res. II* **48**, 3913 (2001).
14. H. M. Sosik, R. J. Olson, *Deep-Sea Res. I* **49**, 1195 (2002).
15. M. R. Hiscock *et al.*, *Deep-Sea Res. II* **50**, 533 (2003).
16. J. L. Hand *et al.*, *J. Geophys. Res.* **109**, D17205 (2004).
17. E. L. Rue, K. W. Bruland, *Mar. Chem.* **50**, 117 (1995).
18. J. F. Wu, G. W. Luther, *Mar. Chem.* **50**, 159 (1995).
19. D. A. Hutchins, A. E. Witter, A. Butler, G. W. Luther, *Nature* **400**, 858 (1999).
20. P. Sprent, G. R. Dolby, *Biometrics* **36**, 547 (1980).
21. E. A. Laws, *Deep-Sea Res. A* **38**, 143 (1991).
22. W. G. Sunda, *Mar. Chem.* **57**, 169 (1997).
23. W. G. Sunda, S. A. Huntsman, *Mar. Chem.* **50**, 189 (1995).
24. R. F. Strzepek *et al.*, *Global Biogeochem. Cycles* **19**, GB4S26 (2005).
25. B. S. Twining, S. B. Baines, N. S. Fisher, *Limnol. Oceanogr.* **49**, 2115 (2004).
26. M. T. Maldonado *et al.*, *Limnol. Oceanogr.* **46**, 1802 (2001).
27. W. G. Sunda, S. A. Huntsman, *Nature* **390**, 389 (1997).
28. S. Blain *et al.*, *Nature* **446**, 1070 (2007).
29. P. N. Sedwick, G. R. DiTullio, *Geophys. Res. Lett.* **24**, 2515 (1997).
30. B. B. Prezelin, E. E. Hofmann, C. Mengelt, J. M. Klinck, *J. Mar. Res.* **58**, 165 (2000).
31. H. J. W. Debaar *et al.*, *Nature* **373**, 412 (1995).
32. E. Bucciarelli, S. Blain, P. Treguer, *Mar. Chem.* **73**, 21 (2001).
33. N. M. Mahowald *et al.*, *J. Geophys. Res. Atmos.* **111**, D10202 (2006).
34. R. S. Robinson *et al.*, *Paleoceanography* **20**, PA3003 (2005).
35. A. H. Orsi, T. Whitworth, W. D. Nowlin, *Deep-Sea Res. I* **42**, 641 (1995).
36. We thank P. Ginoux, M. Reuer, and P. Falkowski for helpful discussions, two anonymous reviewers for perceptive comments, and P. Schultz for providing the average climatological mixed layer PAR data-product. We gratefully acknowledge support for this work from NASA, NSF, the Gary Comer Family Foundation, and the CSIRO Climate Change Research Program.

The Evolution of Selfing in *Arabidopsis thaliana*

Chunlao Tang,[1] Christopher Toomajian,[1] Susan Sherman-Broyles,[2] Vincent Plagnol,[1,3] Ya-Long Guo,[4] Tina T. Hu,[1] Richard M. Clark,[4] June B. Nasrallah,[2] Detlef Weigel,[4,5] Magnus Nordborg[1]*

Unlike most of its close relatives, *Arabidopsis thaliana* is capable of self-pollination. In other members of the mustard family, outcrossing is ensured by the complex self-incompatibility (*S*) locus, which harbors multiple diverged specificity haplotypes that effectively prevent selfing. We investigated the role of the *S* locus in the evolution of and transition to selfing in *A. thaliana*. We found that the *S* locus of *A. thaliana* harbored considerable diversity, which is an apparent remnant of polymorphism in the outcrossing ancestor. Thus, the fixation of a single inactivated *S*-locus allele cannot have been a key step in the transition to selfing. An analysis of the genome-wide pattern of linkage disequilibrium suggests that selfing most likely evolved roughly a million years ago or more.

The transition from outcrossing to selfing is a major theme in the evolution of flowering plants, having occurred independently in numerous lineages (*1*). Although it leads to inbreeding depression, the ability to self can be advantageous when colonizing new territory and is therefore associated with weedy and invasive species. *A. thaliana*, a member of the Brassicaceae,